Chapter 4

Lead Magnesium Niobate

4.1 Introduction

Relaxor ferroelectrics are characterized by a frequency dependent dielectric response which has a broad maximum as a function of temperature. In addition, relaxors possess a local polarization at temperatures above their dielectric maximum. In contrast, "normal" ferroelectrics have a sharp phase transition peak in dielectric constant at their Curie point, and no polarization exists above that temperature. The origin and explanation of relaxor behavior is an ongoing research problem. The prototypical relaxor is lead magnesium niobate, or $Pb(Mg_{1/3}Nb_{2/3})O_3$, which was first synthesized by Smolenskii and Agranovskaya in 1958 [1]. Its dielectric behavior is shown in Figure 3.4. PMN has found applications in a variety of devices where its unique properties have been exploited, even if they are not perfectly understood. Of greatest interest is PMN's very high dielectric constant (~30,000) over a wide temperature range near room temperature.

Lead zinc niobate, or $Pb(Zn_{1/3}Nb_{2/3})O_3$, also has a very high dielectric constant with similar relaxor behavior, but its Curie temperature is 140°C versus -7°C for PMN. PZN has excellent dielectric and piezoelectric properties, especially in solid solutions with lead titanate [2]. Whereas PMN remains cubic down to 5 K [3], PZN undergoes a symmetry change from cubic to rhombohedral at its Curie temperature and is able to

sustain the growth of polar macrodomains[4]. PZN is a somewhat 'new' material, but since the discovery of its very high electromechanical coupling coefficients it has received a lot of attention[2]. Single crystals of PZN and La-doped PZN crystals were grown for this work to compare their behavior to PMN. This chapter focuses on the superstructures found in PMN and PZN, and their relation to the relaxor behavior. Historically, PMN is the more important and widely studied material and will be used in the background discussion. Data collection and analysis procedures were identical for both materials, and the PZN results are included at the end of this chapter.

4.2 Literature review

Both PMN and PZN have the common ABO_3 cubic perovskite structure with a mixed B-site. However, the finer points such as the size and direction of ion displacements within the perovskite model have not been easy to deduce [5,6,7]. This is important because it determines the overall symmetry of the crystal and therefore its ferroelectric behavior. There has been a growing interest in understanding the ordering that occurs at the B-sites. Initially, these compositional fluctuations within nanodomains were believed to create different regions having varying Curie temperatures [8], thus giving PMN its broad relaxor response. Smolenskii [9] proposed that local inhomogeneities in chemistry and/or structure result in microdomains having a distribution of Curie temperatures, leading to a diffuse peak in dielectric constant. However, the situation appears more complicated as La-doped PMN retains its relaxor properties even when micron sized chemically ordered domains form [10] and experiments by Davies, et al, have found relaxor behavior in highly ordered

$Pb(Mg_{1/3}Ta_{2/3})O_3$ and similar systems[11]. As discussed in Chapter 3, theoretical interpretations of relaxors have been offered using various models. A clearer understanding of the charge heterogeneity within PMN and its relation to the ferroelectric domains should help to understand the behavior of this relaxor. Specifically, since the compositional fluctuations on the B-site are believed to be responsible for the relaxor behavior, the effects of both increased and decreased chemical order on the B-site will be studied.

As will be shown, there are two distinct types of domains within PMN, both on the nanometer scale. The ferroelectric nanodomains have local rhombohedral (polar) symmetry and grow only to a maximum of 100 Å [3]. These are the domains that give PMN its ferroelectric behavior, but unlike normal ferroelectrics, they never coarsen into large domains. The limited extent of the polar domains does not allow micron sized domains to form as in normal ferroelectrics. In this work, attention is focused on the second type of nanodomains in PMN which will be shown to be chemically ordered domains. There is an ordering of the B-sites of adjacent unit cells, giving rise to additional superstructure peaks in the diffraction pattern at the (h+1/2, k+1/2, l+1/2) positions. The size of the chemically ordered domains can be varied by doping: substituting La on the Pb site (La-PMN) causes the ordered domain size to be increased. Doping with Ti on the B-site (PMN-PT) causes the ordered domain size to be decreased. The effects of both on the materials' structure and dielectric behavior will be measured.

The existence of a superstructure in PMN was first observed in selected area electron diffraction experiments [12]. Using a transmission electron microscope, superstructure spots were imaged at the (h+1/2, k+1/2, l+1/2) positions. The peaks were relatively weak and broad, suggesting that they originated from limited domain sizes.

Because the half-integer peaks are at the body centered positions in the reciprocal lattice, the symmetry of the superstructure must have a face centered cubic arrangement within a doubled unit cell in real space (space group Fm3m). This work focuses on understanding the structural origin of the superstructure spots in PMN and PZN which could not be deduced from the electron diffraction measurements.

First, the cause of the superstructure peaks must be determined. One type of model that would give superstructure peaks at the (h+1/2, k+1/2, l+1/2) positions is displacement ordering. In this class of models, atoms in adjacent unit cells are displaced in opposite directions, producing a doubled unit cell. If the displacement is Δd, and adjacent atoms are displaced in opposite <111> directions, then the structure factors will have the form:

$$F_{hkl} \propto f \sin(q \cdot \Delta d) \qquad \text{(when h,k,l are integers + 1/2)} \qquad (1)$$

The graph of structure factor, |F|, of the superstructure peaks versus momentum transfer, $|q|$, would initially increase, passing a maximum when $q=\pi/(2\Delta d)$, and then decrease. This was the observation for PMN in the study by Zhang et al [13], and hence they concluded that an ordering in the displacement of ions was producing the superstructure.

4.2.1 Chemical ordering--space charge

Another model that could account for these superstructure peaks involves small regions of 1:1 chemical ordering of the B-site magnesium and niobium ions (Figure 4.1). This was first proposed in TEM studies [14], but could not be verified. The 1:1 ordering found in PMN is somewhat unexpected given the Mg:Nb stoichiometry of 1:2, but it was suggested that this non-stoichiometric ordering may actually help stabilize the perovskite

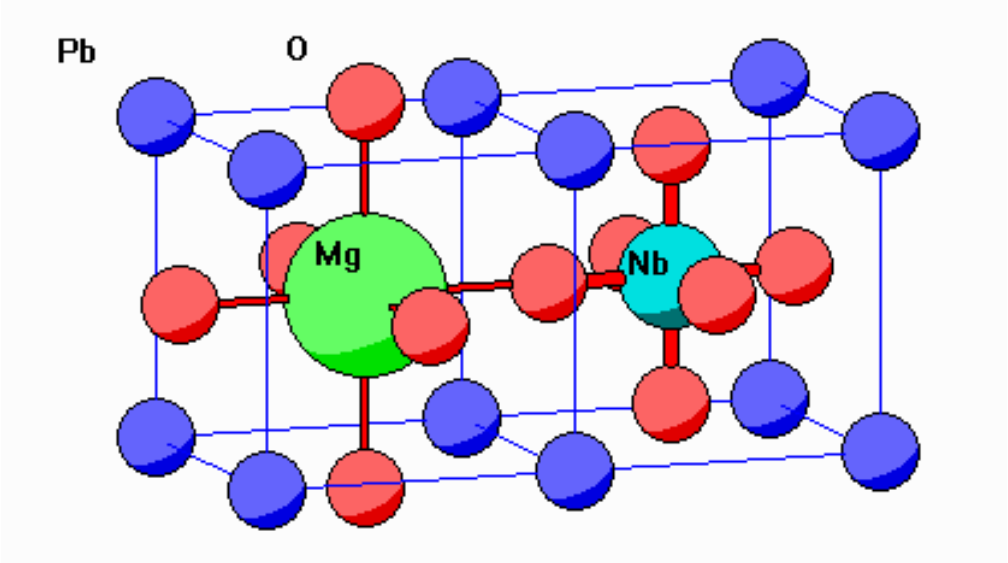

Figure 4.1. Two adjacent unit cells of PMN showing the 1:1 chemical ordering as in the space charge model. In addition, the oxygen displacements in the $R\bar{3}m$ model are shown.

over the pyrochlore structure in PMN[15]. The non-stoichiometric domains would then be

embedded in a sea of Nb rich domains. The ordered domains have a net negative charge which, it was proposed, restricts their size since these domains did not coarsen after annealing at 970°C for extended periods [16]. Chen, Chan and Harmer provided evidence for this model in their study [10]. By doping with La^{3+}, they showed that the size of the ordered domains can be dramatically increased. The La^{3+} ion contributes an extra positive charge compared with the Mg^{2+} thus lessening the charge restriction so the negatively charged ordered domain can increase in size. The opposite effect was seen

when doping with Na^{1+}. Because of the net charge per unit cell, this model is termed "space charge."

4.2.2 Chemical ordering--random layer

A variation of the complete chemical ordering model that maintains charge balance is the "random layer" model [10], in which the 1:1 ordering is between two chemical species, B′ and B′′. The "random layer" model also involves 1:1 chemical ordering, but not a simple Mg-Nb-Mg-Nb ordering. In this model, B′ contains a random occupation of Mg and Nb ions in a 2:1 ratio, while B′′ is always Nb. Thus the B′ site is disordered, while B′′ is ordered, so the superstructure is well-defined. In this extreme case, there would be no charge imbalance and the entire crystal volume could be composed of these ordered domains with the chemical formula: $Pb[(Mg_{2/3}Nb_{1/3})_{1/2}Nb_{1/2}]O_3$. Intermediate situations between the full 1:1 Mg:Nb chemically ordered model and the B′- B′′ model can exist, with different volume fraction of the ordered domains.

The above descriptions result when adjacent unit cells have sites either occupied by different ions or with a preference for different types of ions. Effectively, this doubles the size of the unit cell, producing a superstructure that exists over small domains. A diffraction experiment is a good way to probe the degree of ordering through crystallographic analysis of structure factor measurements. If the two B-site ions have effective atomic form factors f_I and f_{II}, then a simple derivation gives the form of the structure factors as a function of momentum transfer magnitude, $|q|$:

$$F_{hkl} \propto f_I - f_{II} \qquad \text{(when h,k,l are all half-integers)} \qquad (2)$$

So, for chemical ordering models, the intensity of the superstructure reflections depends on the difference in form factor of the two chemical species, and hence gradually decreases as a function of momentum transfer, $|q|$, according to the shape of atomic form factors. In the complete chemical ordering model, this results in F_{hkl} being proportional to $f_{Nb} - f_{Mg}$. In the random layer model, B′ is an average ion of $(Mg_{2/3}Nb_{1/3})$ and B′′ is Nb, so the resulting structure factor is identical except for a factor of 2/3:

$$F_{hkl} \propto f_{Nb} - \left(\tfrac{2}{3} f_{Mg} + \tfrac{1}{3} f_{Nb}\right) = \tfrac{2}{3}\left(f_{Nb} - f_{Mg}\right) \qquad (3)$$

which makes the two chemically ordered models indistinguishable in the diffraction pattern, unless measurements are made on an absolute scale. Compared with the displacement ordering model, however, the behavior is quite different.

Evidence for the "random layer" model in $A(B'_{1/3}B''_{2/3})O_3$ systems was recently reported by Akbas and Davies [11] who found greatly increased ordered domains in $Pb(Mg_{1/3}Ta_{2/3})O_3$ and similar ceramics by annealing to very high temperature (~ 1325°C). This is strong evidence that the "random layer" model applies to that system because the excess electrostatic energy in such highly ordered systems would make the "space charge" model impossible (discussed in Section 4.4.4 below). However, similar annealing experiments for extended periods have failed to coarsen the ordered domains of PMN.

By comparing the superstructure and bulk intensities, Lin and Wu [17] found in powder diffraction experiments that for La concentrations greater than 10%, there is maximum ordering on the B-sites. However, at 10% La content and below the superstructure peaks were very weak. Their plot of lattice constant vs. La content (x) fits a straight line for $x > 10\%$, suggesting complete solid solutions are formed between the

La and Pb atoms. For $x < 10\%$ the lattice constant deviates from the fit, suggesting a more complicated structure. This work focuses attention on the La concentration range below 10%, where the powder diffraction could not give reliable results on ordering. Single crystal X-ray diffraction also can determine the structure of the ordered domain, so atomic displacements can be measured. By doping with La, the effect of increased ordered domain size on the atomic structure and dielectric behavior can be studied. By doping with Ti, the opposite effect of decreased domain size will be examined.

The organization of this chapter is as follows. First, the crystal growth procedure is described. Then, the crystallographic analysis and refinement of the structures for PMN and La-PMN allow the size and structure of the ordered domain to be determined for each sample. Next, the electrostatic energies involved with the various models are estimated and it is seen that the space charge model can not explain the doping trends. An alternative analysis shows that internal strain effects may be driving the chemical ordering. In addition, it is found that the random layer model must be present in the La-doped samples. An interpretation of the relationship between ordered domain size and relaxor behavior is given. Experiments on Ti doped crystals demonstrate the opposite effect of La-PMN and provide further evidence of the interplay between chemically ordered and polar domains. Finally, similar experiments on the PZN system are described to back up the conclusions drawn from the PMN experiments.

4.3 Crystal growth

Crystals of pure PMN and PMN-PT of roughly 2 mm per side were used. These crystals were grown using the Czochralski method [18]. One PMN crystal was as grown,

with well formed <100> faces on three sides. The other PMN crystal and the PMN-PT crystal were cut from larger crystals and polished so that the largest face was <100>. Lanthanum doped crystals were grown for this experiment using high temperature solution growth. First, La-PMN powder was prepared using the columbite method described by Swartz and Shrout [19]. Powders of PbO, MgO, Nb_2O_5, and La_2O_3 with purities exceeding 99.7% were used. When doping with La^{3+} for Pb^{2+}, it is necessary to account for the charge imbalance in one of two ways. By keeping the ratio of Mg:Nb concentration fixed, A-site vacancies can be introduced:

$$Pb_{1-3x/2}La_x\square_{x/2}(Mg_{1/3}Nb_{2/3})O_3$$

where $\square$ represents a vacancy. For this work, however, the Mg:Nb ratio was increased to prevent A-site vacancies, as seen in equations 4 and 5. The columbite phase was produced by heating the magnesium and niobium oxides to 1000°C for 6 hours:

$$\frac{1+x}{3}MgO + \frac{2-x}{3}\frac{1}{2}Nb_2O_5 \rightarrow Mg_{\frac{1+x}{3}}Nb_{\frac{2-x}{3}}O_{\frac{4-x}{2}} \qquad (4)$$

This was then combined with appropriate amounts of La_2O_3 and PbO:

$$\frac{x}{2}La_2O_3 + (1-x)PbO + Mg_{\frac{1+x}{3}}Nb_{\frac{2-x}{3}}O_{\frac{4-x}{2}} \rightarrow La_xPb_{1-x}(Mg_{\frac{1+x}{3}}Nb_{\frac{2-x}{3}})O_3 \qquad (5)$$

The La-PMN powder was then formed by firing to 850 °C for 6 hours. X-ray powder diffraction confirmed the resulting perovskite structure (Figure 4.2). The most common problem with growing PMN is obtaining the pyrochlore structure instead of perovskite. Pyrochlore is a non-cubic, isometric structure with excess oxygen and niobium and its material properties are nothing like perovskite PMN.

Single crystal growth involved combining La-PMN powder with a lead oxide flux. The amount of flux ranged from one to one and a half times the weight of the PMN

powder. The mixture was placed in a tightly covered platinum crucible, and placed in a

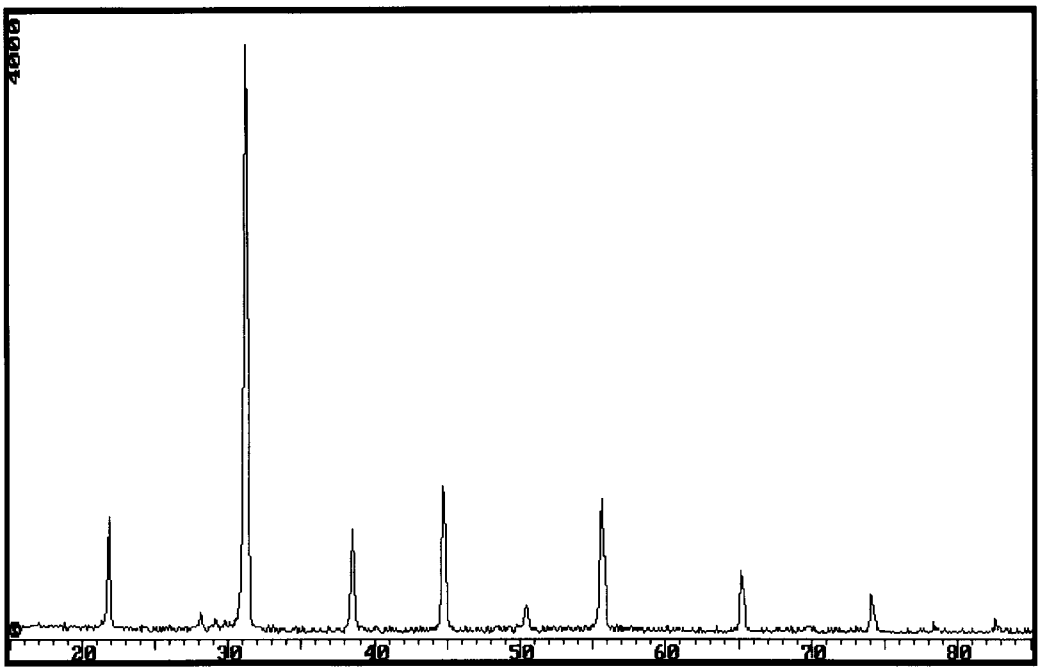

Figure 4.2. Powder x-ray diffraction scan of intensity vs. 2θ for pure PMN with the perovskite structure. After confirming the perovskite structure is present, single crystal growth can be attempted.

larger crucible. Alumina powder surrounded the platinum crucible to help prevent lead loss upon firing. A typical firing schedule involved rapid heating to 1250°C, soaking for 12 hours, then slow cooling at 2° per hour to 1000°C. Cooling continued at 5° per hour to 800°C, and then the mixture was brought to room temperature at 50°per hour. These temperatures were based on the PbO-PMN phase diagram published by Ye et al [20]. The residue was partially dissolved with boiling nitric acid, and single crystals were extracted. In all trials, only small crystals were found. The largest 3% La-PMN crystals were approximately 1 mm per side, while the 10% La-PMN crystals were only about 0.5 mm per side and some were black in color which may have been due to Pt contamination

from the crucible. It was helpful to polish these crystals to give them a well defined, flat face for the X-ray diffraction measurements.

The growth of PZN and La-PZN was easier, as the columbite step was not needed. Appropriate amounts of powder were ball milled and ground, and a PbO flux of one and a half times the La-PZN powder weight was used. The mixture was placed inside a Pt crucible (sealed as above), rapidly heated to 1300°C and then soaked at 1250°C for 12 hours. Single crystal growth occurred under slow cooling at 2° per hour to 800°C. The resulting crystals were on the order of 1.0-1.5 mm per side for both pure PZN and 10% La-PZN, and powder diffraction confirmed the perovskite phase. The irregularly shaped crystals were polished to a flat face for the X-ray and dielectric measurements.

4.4 Lanthanum doped PMN

4.4.1 Measurements

Each crystal was oriented in the diffractometer with one of its flat faces aligned nearly perpendicular to the phi axis [21]. This made it easier to estimate, and hence correct for, the beam's penetration through the crystal at any angle. This face was always close to a <100> orientation, which was designated (001). Measurements were taken at Brookhaven National Laboratory's National Synchrotron Light Source on Beamline X16C. The incoming X-ray beam was tuned to 8.5 keV and focused onto a flat face of the crystal. The beam size was defined by slits to be 1×1 mm. The linear absorption coefficient for PMN at 8.5keV is approximately 1150 cm^{-1}, giving a characteristic penetration depth of 8.7 microns along the beam direction. The detector arm's slits were set at 2x2 mm to define the resolution function. The orientation matrix of the crystal was

determined by measuring several bulk Bragg reflections. The refined lattice parameters were 4.048(2) Å for pure PMN, in agreement with published values [22]. The lattice constants steadily decrease with increasing La concentration, due to the smaller ionic radius of La compared to Pb.

Scans were made to measure the integrated intensities of the (h+1/2, k+1/2, l+1/2) superstructure peaks. Because of the big differences in domain size, and hence peak profile, two different methods were needed. The well-ordered crystals (10% La doping) used conventional rocking curves in theta. The less well-ordered samples were measured by reciprocal lattice scans varying one of the indices (Figure 4.3). These peaks were much

broader than the resolution function, so it was necessary to integrate them in three dimensions. Initially, separate measurements along the h, k and l directions were made, but since the widths (in reciprocal lattice units) for each direction were approximately constant and independent of the direction scanned, it was sufficient to scan in only one direction. The integrated intensity was measured as the area under the peak minus the interpolated background. After adjusting for the counting time and the step size in *h*, the intensities were corrected for absorption as described in the following section. Taking the square root gave a measurement that was proportional to the absolute value of the structure factor, |F|.

Dielectric data were also measured for the La-PMN crystals. The dielectric response was recorded using a Hewlett-Packard (HP) 4284A inductance-capacitance-resistance (LCR) bridge, which can cover a frequency range between 20 and 10^6 Hz. For low temperature measurements, the samples were placed in a Delta Design 9023 test

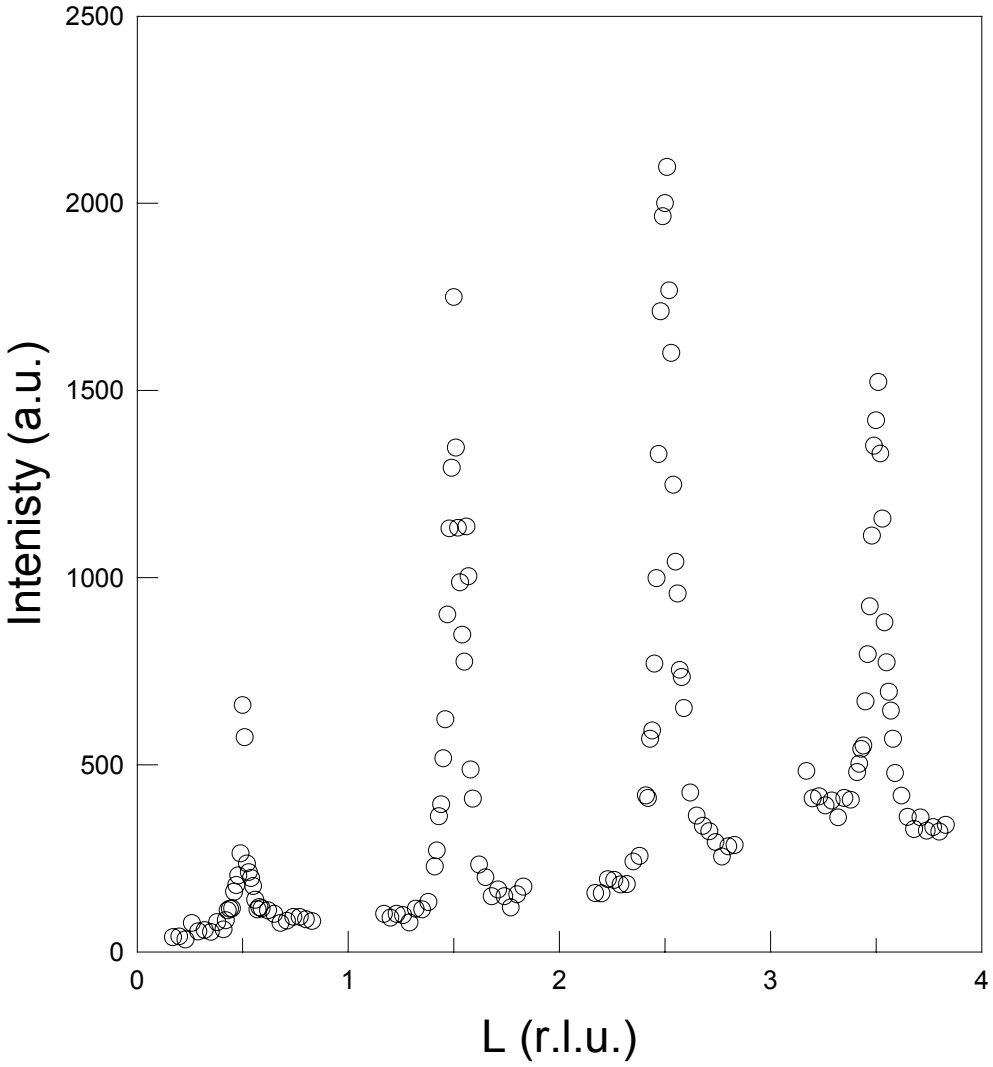

Figure 4.3. Raw x-ray diffraction data showing the intensities of four adjacent superstructure peaks. Scanned in the Miller index l, with h = k = 0.5.

chamber. The temperature was measured using a HP 34401A multimeter, via a platinum resistance thermometer mounted directly on the ground electrode of the sample fixture. The complex dielectric constant function is written as: $\varepsilon = \varepsilon' + i\,\varepsilon''$ where ε' is the DC dielectric constant, and ε'' is the dielectric loss. Measurements were performed on cooling, using a rate of 2º per minute at different frequencies. The results for the La-doped samples are presented in Figure 4.4, with measurement frequencies from 1 to 500 kHz. By doping with La^{3+}, the dielectric constant $\varepsilon'(T)$ peak becomes broader and its maximum value decreases dramatically compared to pure PMN (Table 4.1). Doping with La causes the peak in the dielectric constant to move to lower temperatures. Typical of relaxors, as the measurement frequency increased, the peak decreased and shifted to higher temperatures with dispersion in ε' and ε''. ε' decreased with increasing frequency on the low temperature side of the peak, whereas ε'' increased with increasing frequency on the high temperature side of the peak, characteristic of relaxor behavior. At higher temperatures, (~ 350 K) the decrease in ε'' observed with increasing frequency can be attributed to thermally stimulated conductivity effects, i.e. charge transport rather than local charge displacements, possibly due to the small size of the crystals. The frequency dependence shows a larger frequency dispersion than pure PMN, indicative of more relaxor like behavior.

Table 4.1. Summary of domain size and dielectric constant data measured for the samples with different La^{3+} doping concentrations. Increases in La^{3+} led to much larger ordered domains and smaller dielectric constants.

Sample	avg. FWHM ($Å^{-1}$)	Domain size (Å)	ε' max. at 1 kHz	Temp. (C) of ε' max.
PMN I	0.124	47		
PMN II	0.118	50	30,000	-5.0
3% La-PMN	0.0746	130	7,600	-45.0
10% La-PMN	0.00647	910	1,200	-63.0

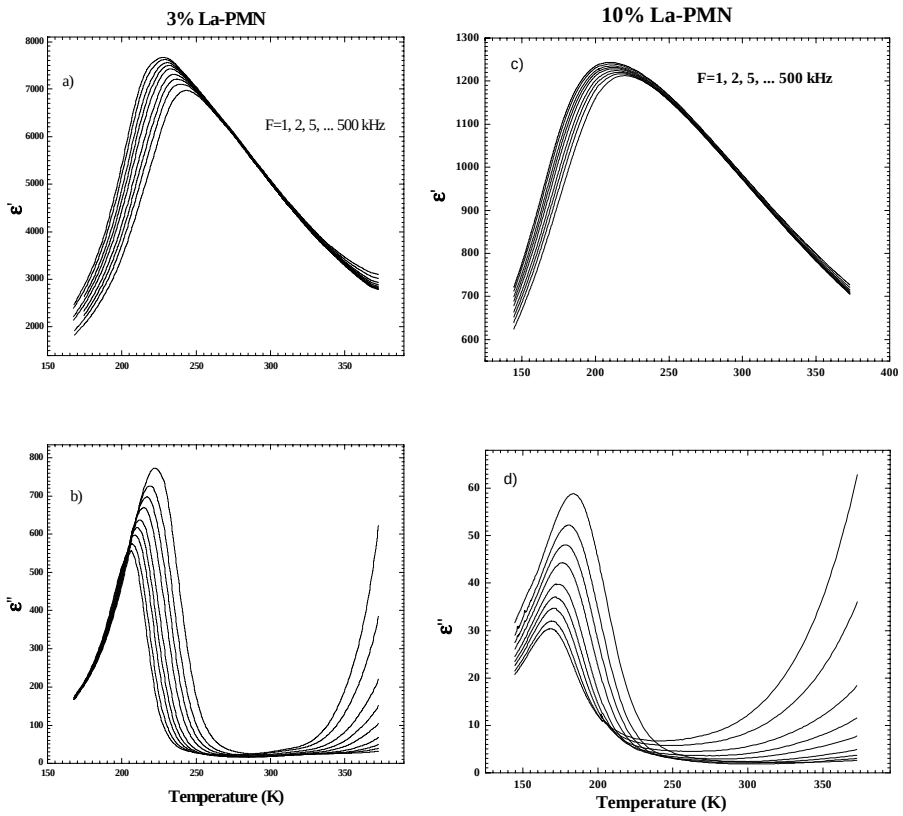

Figure 4.4. Dielectric constant, ε′, (a,c) and loss, ε′′ (b,d) measured on the 3% (a,b) and 10% (c,d) La-PMN crystals as a function of temperature. Measurement frequencies range from 1 to 500 kHz and increase from left to right in each graph.

4.4.2 Analysis

The symmetry and structure of the parent crystal is assumed to be ideal cubic perovskite. By crystallographic analysis of peaks of the form (h+1/2, k+1/2, l+1/2), the nature of the superstructure can be determined and hence the mechanism of ordering. Approximately 150 superstructure reflections were measured for each crystal. For each reflection, at least four symmetrically equivalent peaks were measured (e.g. ±0.5, ±0.5, 0.5). Only peaks with $\chi > 30°$[21] were measured to keep the entrance and exit beams passing through the alignment face. By averaging over the symmetrically equivalent scans, the 150 measured peaks were reduced to 19 crystallographically distinct reflections (of a possible 21 below the two-theta limit). This was a sufficient number to determine the structure of the ordered domains and observe changes with La or Ti doping. The agreement within the symmetry equivalent peaks was best for the larger pure PMN crystals at 7.8%. For 3% La-PMN, it was 14.1%, for 10% La-PMN it was 18.1%, and for 6% PMN-PT it was 8.1%. The larger errors are most likely due to the smaller crystal size and ill defined faces in the La-PMN which introduced errors through the absorption correction.

The general shape of the raw data agrees with that of Zhang et al [13], in that it appears to show a sinusoidal variation with $|q|$ (Figure 4.3). This suggests a displacement ordering model. However, there are important corrections needed to deduce structure factors from the raw data which change the conclusions significantly. The absorption of the beam as it passes through the Pb-rich sample must be accounted for. The size of the

beam (~1 mm) is slightly smaller than the pure PMN crystals and larger than the La-doped

samples. At angles above a threshold incidence angle, the entire beam hits the pure PMN crystal. This is the extended face regime in which the integrated intensity is shown by Warren [23] to be proportional to:

$$\int_{z=0}^{\infty} e^{-2\mu z/\sin\theta} \frac{A_0 dz}{\sin\theta} \tag{6}$$

This assumes an "infinitely" thick crystal and a beam whose footprint is smaller than the crystal's horizontal dimension. Here μ is the absorption coefficient, A_0 is the area illuminated, θ is the incident angle, and z is the penetration of the beam into the crystal. The integral evaluates to $1/2\mu$, so the effect of absorption is just a constant factor because even though it increases with increasing path length at smaller incidence angles, the illuminated area of the crystal also increases.

However, below that threshold angle (and at all angles for the smaller crystals), the extended face geometry is no longer valid because the beam footprint is now larger than the crystal. The absorption must be accounted for by adjusting for the fraction of the beam that is illuminating the crystal which depends on the incidence angle, α_i. This illumination correction is given by $1/\sin(\alpha_i)$, or $1/\sin(\theta)\sin(\chi)$, which is the footprint of the beam on the sample following the angle convention of Busing and Levy [21] when the flat face of the sample is perpendicular to the phi axis. This correction is significant for structure factors measured at low incidence angles and mostly affects the low $|q|$ reflections. The extended face absorption correction has to be adjusted because some fraction of the beam never hits the crystal. This illumination correction is only valid for

crystals with a flat face, and when the x-rays that reach the detector enter and exit through that face symmetrically as was the case in these measurements. Because of the large absorption of PMN, most radiation entering a side of the crystal would not contribute to the intensity anyway. Initially, the smaller 10% La-PMN crystals were studied in their as-grown, jagged state. Large errors were found in the scattering intensities in that symmetrically equivalent peaks had very different intensities. By polishing the crystal down to a flat face, this problem was largely eliminated.

The width of an X-ray peak is inversely proportional to the size of the domain that is contributing to that particular scattering event as given by the Scherrer formula:

$$L = 0.94 \frac{2\pi}{\Delta q_{FWHM}} \tag{7}$$

where L is the characteristic length of the ordered region and Δq_{FWHM} is the peak width measured in reciprocal space. By measuring the widths of half-order superstructure peaks, it is therefore possible to estimate the size of the ordered region. The average size of the domains that caused the superstructure peaks was 48 Å for both pure PMN samples, based on an average width of 0.12 $Å^{-1}$. The peak widths for various reflections were constant when measured in momentum transfer units (rather than angle) which indicated that the width was entirely a finite-size effect and had little contribution from the sample mosaic spread.

For the La-doped case, there was a dramatic increase in ordered domain size with increasing La doping (Table 4.1). The 10% La concentration produced ordered domains of approximately 900 Å. The peaks were so narrow that they were close to the limits of resolution, which is why the θ-scan integration method was used. In the 6% PMN-PT sample, the opposite effect was seen and the ordered domains were only on the order of

30 Å per side. Very faint superstructure reflections were also observed in 10% PMN-PT

but were too weak to do a complete analysis. This is closer to the morphotropic phase boundary where PMN-PT changes from a relaxor to a normal ferroelectric and the chemically ordered domains disappear.

4.4.3 Results

The absorption corrected data show a very different q-dependence from the raw data (Figure 4.5). The graph of structure factor vs. $|q|$ follows the monotonic decay (similar to the shape of atomic form factors) that is characteristic of the chemical ordering models. This was true for all the crystals that were studied. Using a simple chemical

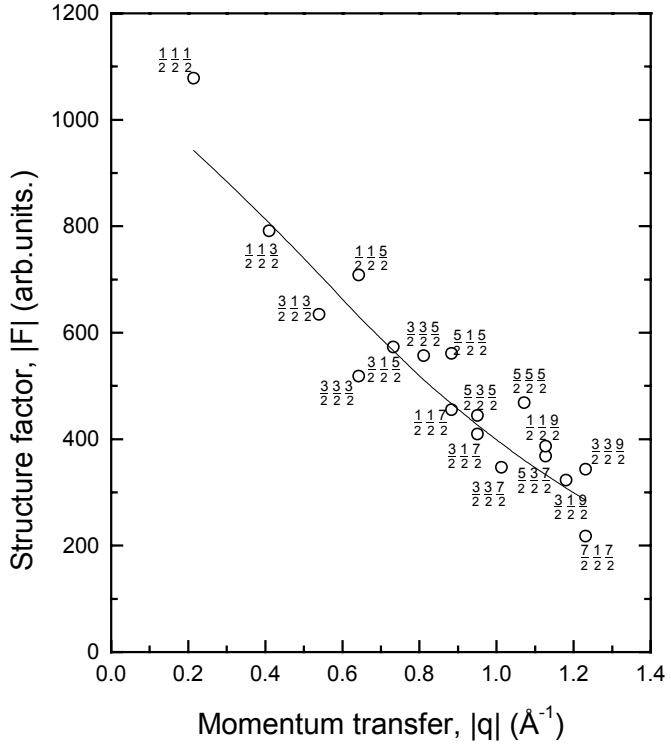

Figure 4.5. Structure factors (after corrections) vs. momentum transfer for superstructure reflections of pure PMN. The fit is to a simple chemical ordering model with no displacements..

ordering model, it is possible to fit the general shape of the data (line in Figure 4.5). However, chemical ordering alone gives the smooth line of the form factor difference between Mg^{2+} and Nb^{5+} (eqn. 2), and is not able to explain the small, systematic variations seen in the data. For example, certain pairs of reflections, with different indices but the same magnitude of $|q|$, have different structure factors. This simple fit results in a large chi-squared of 3.6.

By varying the position or shape of the oxygen octahedra that surround the B sites, it was possible to fit the deviations from the smooth curve. One such model, with $R\bar{3}m$ symmetry, was suggested by Husson et al [24] in a study of other perovskites, and a similar model was used to fit the data presented here. For the sake of simplicity, complete 1:1 chemical ordering between the B-site ions within each ordered domain ("space charge" model) was assumed, but the model would apply equally well to the charge balanced random layer model since the structure factors only differ by a multiplicative factor as explained above. Because there is no absolute scale factor in the model and the oxygen displacement is a small perturbation of the structure, the degree of 1:1 ordering on an absolute scale could not be measured. In the $R\bar{3}m$ model, the oxygen atoms move towards the smaller Nb^{5+} ions along a {100} axis (and hence move away from the Mg^{2+} ions) (Figure 4.1). This oxygen displacement enabled the model to fit variations in structure factor for reflections that have the same magnitude of $|q|$, for example reflections (1.5, 1.5, 1.5) and (0.5, 0.5, 2.5). By fitting only the size of this oxygen displacement and assigning Debye-Waller factors to the Mg/Nb and O atoms, an

optimal oxygen displacement of 0.044(3) Å for pure PMN was found. The improved fit (Figure 4.6) has a

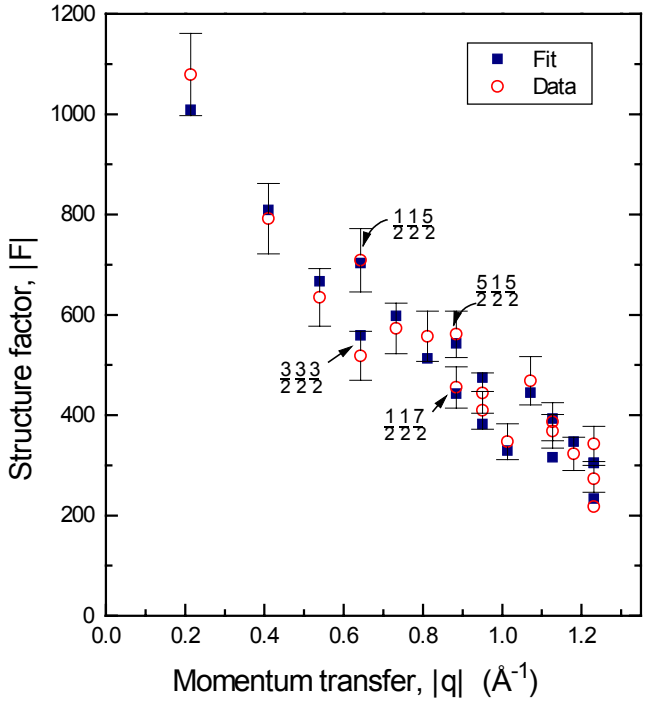

Figure 4.6. Improved fit using the $R\bar{3}m$ model and an oxygen displacement of 0.044 Å. This same model was also used to fit the doped PMN samples.

χ^2 of only 0.6. Models involving rotations of the oxygen octahedra were also attempted but they did not improve the fit. The same model was used to fit the data for the doped crystals. The resulting oxygen displacements are graphed in Figure 4.7 together with the lattice constant dependence. The chi-squared values were 0.9 for 3% La-PMN and 1.2 for 10% La-PMN. The 6% PMN-PT had an oxygen displacement of 0.024 Å, similar to 10% La-PMN, with a chi-squared of 1.4. The direction of the displacement in each case

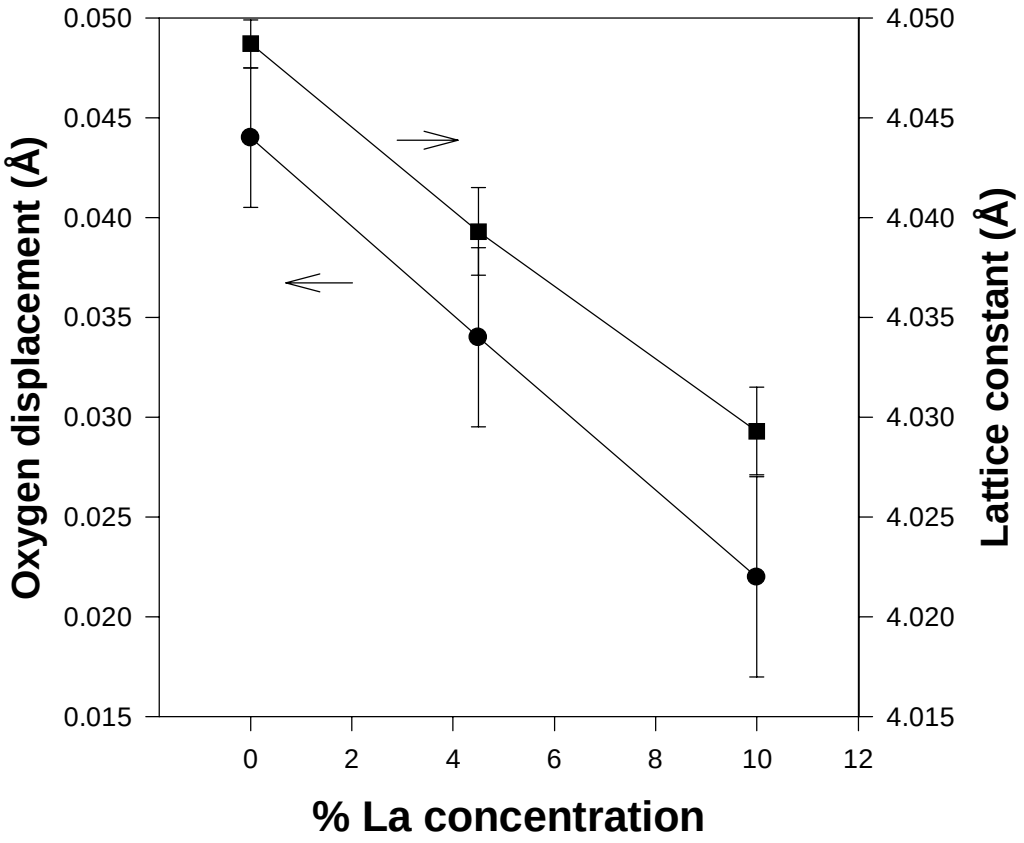

Figure 4.7. Oxygen displacement and lattice constant as a function of La doping. The displacement was found by fitting to the $R\bar{3}m$ model and is towards the Nb or B´´ site.

rays to oxygen, additional oxygen rotations cannot be ruled out. However, the important result is the observed shrinking of oxygen displacements with increasing La doping.

These results indicate that chemical ordering is the dominant cause of PMN's superstructure peaks. The ordered domains have an average size of 48 Å per side and were not strongly anisotropic, so it is assumed they are roughly cubic in shape. These chemically ordered domains are believed to be distinct from PMN's nanopolar domains because they have different characteristics. The superstructure peaks that arise from the

ordered domains showed no response to applied electric fields up to 2 kV/cm in our experiments, and they are also unaffected by temperature up to 1325°C [25]. The nanopolar domains, which appear when PMN is cooled, grow in size when temperature is lowered and are responsible for PMN's ferroelectric properties. Chemically ordered domains are not affected by temperature, increase with La doping and their growth causes a decrease in the dielectric response (Figure 4.4). Doping with Ti (Section 4.2) causes the volume of polar domains to grow as PMN becomes more like a normal ferroelectric. This growth is accompanied by a decrease in the ordered domain size, again showing the competition between two different types of nanodomains in PMN.

Contrary to experiments on other mixed B-site relaxors [26], the increased B-site ordering in PMN results in more relaxor-like behavior as seen in the increased dispersion and broader peak of dielectric constant. It appears that PMN's relaxor behavior is not dependent on the heterogeneity of the B-site but rather the interference caused by the two types of nanodomains. The polar nanodomains' inability to coarsen into larger domains gives PMN its relaxor behavior. As the chemically ordered domain size increases (through La doping), the separation between the polar domains must also increase. The added frustration then increases the relaxor behavior, as observed in the dielectric measurements. In addition, the increase of ordered domains occurs at the expense of the total volume of polar domains as seen in the reduced maximum dielectric constant. Conversely, as Ti is added, it is observed that the maximum dielectric constant increases while the ordered domain size decreases. The result is that PMN begins to behave more like a normal ferroelectric as the interference of the chemically ordered domains is removed. Thus, the relaxor behavior can be understood as resulting from frustration of the polar nanodomains caused by the domains of chemical ordering. Increasing the

chemically ordered domain size results in increased relaxor behavior, while decreasing it leads to decreased relaxor behavior. For lead titanate concentrations above 30%, PMN-PT transforms to a normal ferroelectric and the superstructure peaks are no longer present.

4.4.4 Charge imbalance models

In this section, the question of "space charge" vs. "random layer" model will be considered. The space charge model of complete chemical ordering is only possible for limited domain sizes because there is in fact twice as much Nb as Mg in the chemical composition of PMN. More importantly, the 1:1 Mg:Nb stoichiometry leaves a net charge per unit cell of -0.5*e*. Assuming the domain shape is cubic, the net charge of the cube can be calculated:

$$\text{Volume} = h^3 \qquad Q = \left(\frac{h}{a_0}\right)^3 (-0.5e) \tag{8}$$

This net negative charge can be balanced by a surface layer of positive charge on the unit cells that enclose the ordered region. If such a layer were made up of unit cells of $PbNbO_3$, than each surface unit cell would have a net positive charge of +*e*. By setting the surface layer charge equal to the volume charge, it is seen that 12 unit cells along each cube dimension are needed to achieve charge balance:

$$\left(\frac{h}{a_0}\right)^3 (0.5e) = 6\left(\frac{h}{a_0}\right)^2 (1.0e) \qquad \frac{h}{a_0} = 12 \tag{9}$$

With a lattice constant of 4.048 Å, this region would be 48.6 Å per side. Thus, the observed domain size of 48 Å in pure PMN is the minimum necessary so that one monolayer of unit cells of $PbNbO_3$ will counterbalance it. If this model is correct, then it

can be concluded that these domains do not grow larger because they are strongly restricted by Coulombic forces.

The amount of electrostatic energy contained in such a charge imbalanced region of a crystal can be calculated in a straightforward manner [27]. Consider a spherical volume of radius R containing a total charge Q uniformly distributed in a medium of relative dielectric constant ε_r. Again, a skin charge which counterbalances the volume excess charge and hence cancels all fields outside the sphere is assumed. The electrostatic energy is given by:

$$U = \frac{1}{10}\frac{Q^2}{4\pi\varepsilon_r\varepsilon_0 R} \tag{10}$$

Now, if there are N unit cells in the volume, each with an excess charge q, then $Q=N^3q$ and $R=Na_0$. Substituting gives:

$$U = \frac{1}{10}\frac{\left(N^3 q\right)^2}{4\pi\varepsilon_r\varepsilon_0\left(Na_0\right)} = \frac{1}{10}N^5\frac{q^2}{4\pi\varepsilon_r\varepsilon_0 a_0} \tag{11}$$

The energy per unit cell is then given by:

$$u = \frac{U}{N^3} = \frac{1}{10}\frac{N^2}{\varepsilon_r}\left(\frac{q}{e}\right)^2(3.6eV) \tag{12}$$

This gives $(13/\varepsilon_r)$ eV per unit cell in pure PMN, assuming $N = 12$ unit cells in the ordered region and complete chemical ordering (q=0.5e). Considering ε_r may be quite large, this energy is certainly not unreasonable on the scale of typical cohesive energies of ionic solids. The actual value of ε_r, which is the dielectric constant of the ordered region, is not known, but an approximation of about 100 can be made by extrapolating the Curie Weiss law to PMN's growth temperature. This results in $u \sim 0.13$ eV/unit cell for full chemical ordering in pure PMN.

It was proposed [10] that doping the Pb^{2+} sites with La^{3+} provides enough additional positive charge to allow these domains to become larger. However, at the quantitative level, doping with La does not provide enough positive charge to account for the rapid increase in the ordered domain size. Assuming that the La is distributed evenly on the A-sites, then the net charge for one formula unit of $La_xPb_{1-x}Mg_{0.5}Nb_{0.5}O_3$ is (x-0.5) electrons per unit cell. As above, the number of unit cells per side of the ordered region is:

$$\left(\frac{h}{a_0}\right)^3 (0.5-x)e = 6\left(\frac{h}{a_0}\right)^2 (1.0e) \qquad \frac{h}{a_0} = \frac{6}{0.5-x} \qquad (13)$$

which has a weak dependence on x, giving only 15 unit cells, or 61 Å for 10 % La doping, which is nowhere near the observed 900 Å. It is possible that La goes preferentially into the ordered domains during growth, but no evidence for this was seen in comparing lattice constants of bulk and superstructure peaks.

The conclusion is that the "random layer" model is valid for sufficient La concentrations when the ordered domains are very large, but the "space charge" model is possible in the range below a few percent. Also, it is possible that the anomalous variation of lattice constant for La concentration less than 10% in the measurements of Lin and Wu [17] may indicate a transformation from "space charge" to "random layer" ordering.

4.4.5 Strain effect

A comprehensive explanation for why PMN chemically orders has not yet been given. The structural results presented above indicate that strain plays an important role. In perovskites, there is a delicate balance between ionic contacts at the A and B-sites. The relevant ionic radii, which vary with effective ionic charge and coordination number, are given in Table 4.2 [28]. In pure PMN, the lattice constant is 4.048 Å which, after accounting for two oxygen radii of 1.35 Å, leaves enough room to accommodate a B-site ion of radius 0.674 Å or smaller. Thus, the Nb^{5+} ion fits easily, but the Mg^{2+} ion is too large. However, by constructing a linear array of Nb^{5+} and Mg^{2+} ions (as in a 1:1 chemically ordered model) and displacing the oxygen atoms towards the smaller Nb ion, the Mg ion can be comfortably accommodated. The measurements of oxygen displacements are entirely consistent with this model. The combination of chemical ordering, with the associated oxygen displacements, may lower the total energy by reducing the strain and thereby drive the 1:1 chemical ordering. Doping with La^{3+} decreases the lattice constant, thereby increasing the internal strain by increasing the packing forces. This could make the chemically ordered state even more advantageous in

Table 4.2. Ionic radii from Shannon [28].

	Charge	Coord.	Radius (Å)
Pb	+2	12	1.50
La	+3	12	1.32
Mg	+2	6	0.72
Nb	+5	6	0.64
Ti	+4	6	0.60
O	-2	2	1.35

energy and result in increased ordering in La-PMN. In Chapter 5, an external strain is applied to PMN by growing thin films on a substrate that has a smaller lattice constant. In those measurements, the external strain also had the effect of increasing the ordered domains without having to dope with La.

As the overall lattice constant decreases with increased La^{3+} content, the size of the oxygen displacement also decreases (Figure 4.7). Both curves are on the same vertical scale, so it is seen that the two values change at an approximately equal rate. Using a hard sphere model and the ionic radii (Table 4.2), O-Nb-O requires 3.98 Å and O-Mg-O

requires 4.14 Å. In pure PMN, using the measured oxygen displacement, the O-Nb-O bond length is 3.96 Å, and the O-Mg-O bond length is 4.14 Å, so that the Nb ion is being squeezed slightly, but the Mg ion fits exactly. As La is added, the data indicate that the measured O-Nb-O bond length remains approximately constant at 3.97 Å, while the O-Mg-O bonds become progressively more compressed. The displacements are such that the O-Nb-O distance is roughly constant, and all of the strain is concentrated in the O-Mg-O bond (Figure 4.8).

This result makes little sense in the context of a fully 1:1 Mg:Nb chemically ordered model. It makes more sense if the B′, or 'Mg,' site is showing a change of composition with La doping. The smaller bond length may force the larger Mg out of the B′ site, increasing the amount of Nb on B′. This brings the ordered domains closer to neutral charge because of the additional positive charge carried by Nb^{5+} on the B′ site. In other words, the ordered domain changes from complete Nb:Mg ordering in pure PMN and becomes closer to random layer ordering of Nb:($Mg_{2/3}Nb_{1/3}$) in 10% La-PMN. By this mechanism, the domain size is no longer limited by "space charge" and can grow

larger. Also, because of the quadratic dependence of u on N (eqn. 12), the electrostatic

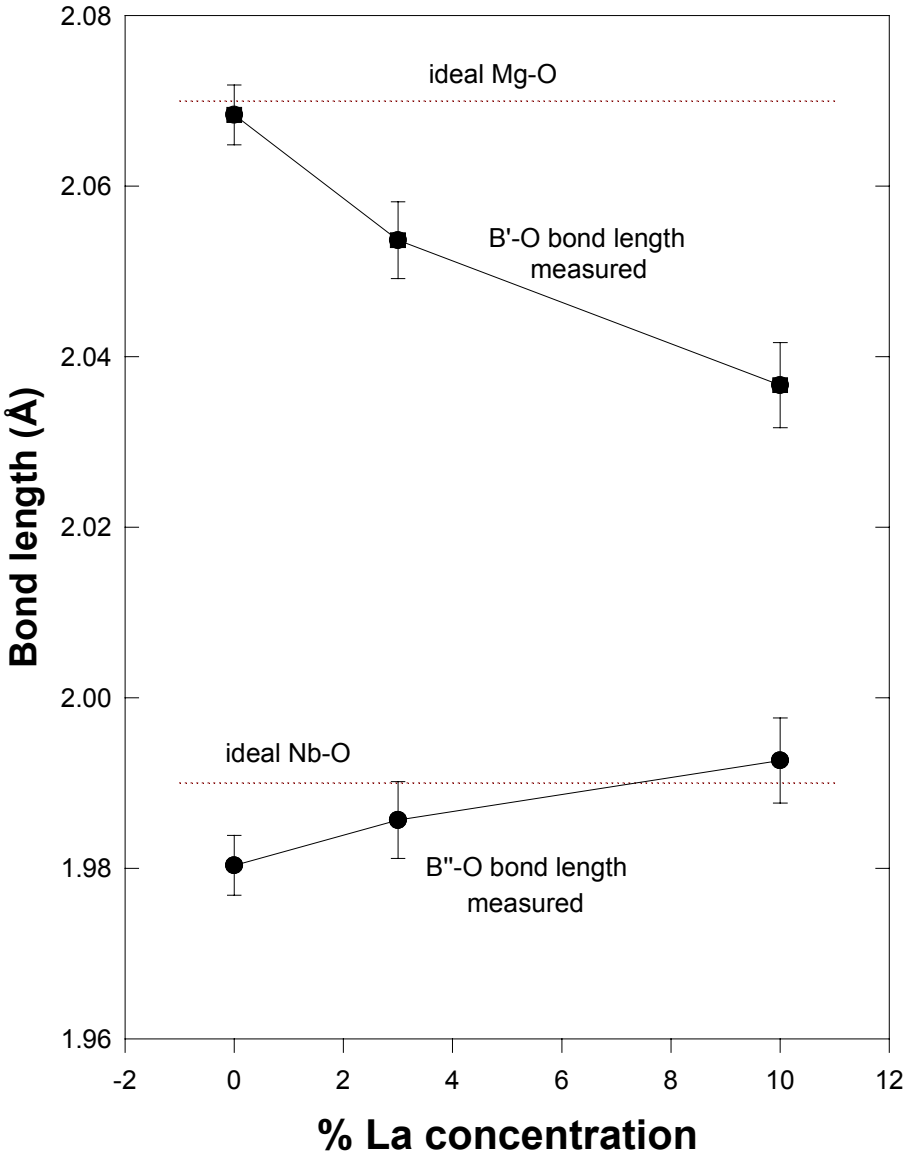

Figure 4.8. Calculated bond lengths of B′-O and B′′-O as a function of La doping. In pure PMN, both Mg on the B′ site and Nb on the B′′ site can be accommodated, but as La is added, the B′ site is squeezed suggesting a change in occupancy from pure Mg to a mixture of Mg and Nb.

energy becomes prohibitively large when *N* becomes larger. Hence, the charge redistribution on the B-sites is necessary to accommodate the large ordered domains in La-PMN.

The data can be interpreted using the model of changing stoichiometry to accommodate the shrinking B′ site. Using the measured lattice constants, a_0, and oxygen displacements, D_{Oxy}, the space allowed for the B′ ion, R_B, is simply:

$$R_B = a_0/2 - R_{Oxy} + D_{Oxy} \qquad (14)$$

where R_{Oxy} is taken from Table 4.2. A linear combination of the ionic radii, R_{Mg} and R_{Nb}, results in an effective radius. An independent estimate of the B′ occupancy is made by calculating the fractions of Mg and Nb that result in an ion that matches the measured size:

$$R_B = y\,R_{Mg} + (1-y)R_{Nb}, \text{ giving} \qquad y = \frac{R_B - R_{Nb}}{R_{Mg} - R_{Nb}} \qquad (15)$$

The results (Table 4.3) show good agreement for the pure PMN and 3% La-PMN, which have Mg occupancies of 0.98 and 0.79 respectively. For the 10% La-PMN, the Mg occupancy actually drops below the random layer model value of 2/3 (which would make the domain positively charged) but the value of 2/3 is still within the error estimate.

Table 4.3. R_B is the measured ionic radius that would fit in the B′ site. The fraction of Mg, in combination with Nb, that corresponds to that size and the resultant excess charge per unit cell are shown.

% La in PMN	R_B measured (eqn. 16)	Mg fraction on B′ site, *y* calc. (eqn. 17)	charge/unit cell *q/e* calculated
0	0.718±0.003	0.98±0.04	-0.46±0.06
3	0.704±0.004	0.79±0.06	-0.19±0.08
10	0.688±0.005	0.60±0.08	+0.10±0.12

Alternatively, the change in bond length could be due to the effects of the La dopant and/or the increased Mg:Nb ratio.

4.5 Titanium doped PMN

In the 6% PMN-PT crystals, the measured lattice constant was 4.033 (2) Å. This crystal was cut from a larger crystal and had a large polished face. Very good agreement of 6.7% was found within the symmetry equivalent peaks after making the corrections as described above for PMN. The same model was used to fit the data with a resulting oxygen displacement of 0.024(5) Å. These measured values give a B′ site that is 0.69 Å and a B′′ site that is 0.64 Å. These values are also consistent with a "random layer" model with a Mg occupancy on the B′ site of 63%. Apparently, the perturbation introduced by the Ti dopants (and the increased disorder on the B-sites) encouraged a random layer ordering, but over a smaller domain size. In the work of Davies et al [11], it was also found that small dopant levels led to greatly increased ordered domains after annealing and hence random layer ordering (the only type possible in large domains). Apparently the random layer ordering is preferred or more stable in these systems, but it must be induced by adding a dopant. It is possible that the ordered domains in PMN-PT could be increased in size by annealing to very high temperatures as was seen in [11].

In the as-grown crystals studied here, the ordered domain size was only about 30 Å. This again suggests the competition between polar nanodomains and chemically ordered domains. As lead titanate is added to PMN, it becomes more like a normal ferroelectric with a larger dielectric response. This occurs at the expense of the ordered domains which in pure PMN interfere with the polar domains and give it the relaxor

behavior. The growth in dielectric constant and reduced relaxor behavior with the addition of PT is clearly seen in Figure 4.9 from Colla et al [29]. In Figure 4.9a, the transition region becomes narrower with increasing PT content, and Figure 4.9b demonstrates the reduced frequency dispersion with increased PT.

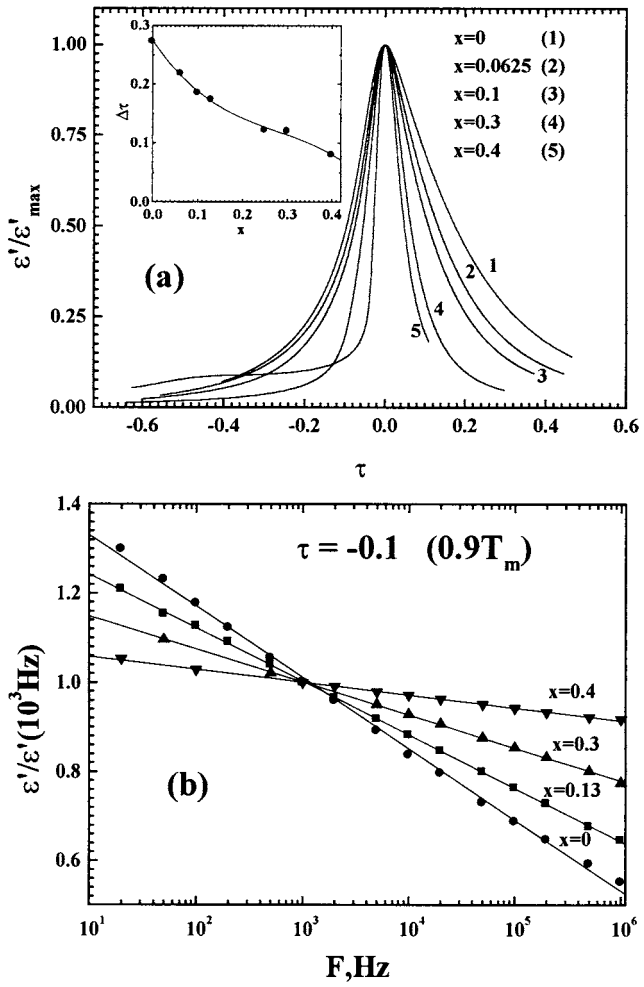

Figure 4.9. Dielectric behavior of PMN-PT for increasing amounts of lead titanate [30]. In a), the transition is seen to become narrower, and in b), the dispersion amount is reduced with increasing PT--becoming less relaxor like. τ is the reduced temperature, or $(T-T_C)/T_C$.

4.6 Lead zinc niobate

Dielectric data were measured for PZN and 10% La-PZN crystals using the same setup discussed above, and the results are presented in Figure 4.10. By doping with La, the ε′(T) peak again became broader and its maximum value decreased significantly. The La also caused the peak in the dielectric constant to move to lower temperatures. Typical

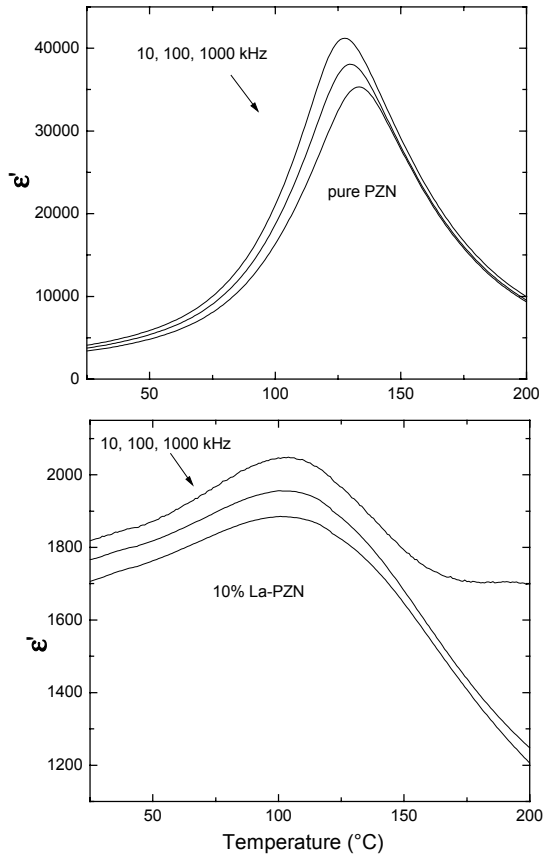

Figure 4.10. Dielectric constant behavior of PZN and 10% La-PZN. As with PMN, La doping leads to larger chemically ordered domains, reduced dielectric constant and increased dispersion (more relaxor like).

of relaxors, as the measurement frequency increased, the peak maximum decreased and shifted to higher temperatures. Again, the La dopant caused more relaxor-like behavior

as seen in the broader transition and greater frequency dispersion. The refined lattice parameters were 4.062(2) Å for pure PZN, and 4.049(2) Å for 10% La-PZN.

Integrated intensities of the (h+1/2, k+1/2, l+1/2) superstructure peaks of 10% La-PZN crystal were measured using theta scans. For 10% La-PZN, 90 such reflections were measured which resulted in 15 crystallographically distinct reflections after averaging symmetrically equivalent peaks. As with PMN, the observed drop off in structure factor with increasing momentum transfer indicated that chemical ordering was the dominant cause of the superstructure peaks in both PZN and 10% La-PZN. However, since the structure factor of chemical ordering superstructure peaks is proportional to the atomic form factor difference (eqn. 2), the PZN peaks from similar domain sizes would be seven times weaker compared with PMN (the form factor difference is 11 electrons between Zn and Nb versus 29 for Mg and Nb).

Using the Scherrer formula, the domain size of PZN was measured to be 25 Å versus the 50 Å found in PMN. This eight times smaller domain volume (without a significant increase in the number of domains), together with the smaller form factor difference, resulted in much weaker superstructure peaks for PZN compared to PMN. As a result, it was not possible to measure enough peaks to do a reliable crystallographic analysis. For the La-doped crystals, there was again a dramatic increase in ordered domain size, so it was possible to model the 10% La-PZN structure. The average ordered domain size of 10% La-PZN was 1200 Å, slightly larger than the 900 Å found for 10% La-PMN.

For 10% La-PZN, the $R\bar{3}m$ model was again used to fit the data. An oxygen displacement of 0.050(6) Å was found, considerably larger than the 0.022(3) Å that was

measured for 10% La-PMN. This larger displacement is expected given that Zn has an ionic radius that is 0.03 Å larger than Mg [28].

Analogous to PMN, it is possible to lend insight to what might be driving the chemical ordering in PZN by considering atomic size. As discussed above, only the random layer model is possible in the highly ordered La-doped crystals because of electrostatic considerations. In the random layer model for 10% La-PZN, the B′ site of $Zn_{2/3}Nb_{1/3}$ has an average radius of 0.72 Å, and the B′′ site (Nb) has an ionic radius of 0.64 Å. The measured lattice constant and oxygen displacement result in an allowed B′ site of 0.72 Å and an allowed B′′ site of 0.62 Å. Thus, the measured oxygen displacement was within 0.01 Å of a "perfect fit," and the system could reduce internal strain by chemically ordering and displacing the oxygen ions.

PZN crystals doped with lead titanate were also grown and measured. As with PMN, the addition of lead titanate to PZN destroys the chemical ordering on the B-sites. Compositions near PZN-9% PT exhibited no half-order peaks. This composition sits on the morphotropic phase boundary above which PZN-PT behaves like a normal ferroelectric. As with PMN-PT, it was observed that the transition from relaxor to normal behavior is accompanied by the disappearance of the half-order peaks and hence the chemically ordered domains. Attempts were made to dope the PZN-PT with La to see if the superstructure could be restored. La dopants of 5, 10 and 20% were added to PZN-9% PT, and in each case the superstructure peaks were still found to be absent. This is further evidence that the drive to chemically order is related to strain effects. Adding smaller Ti ions frees up more space for the larger Zn and Nb ions. So, by reducing the internal packing strain, the drive to chemically order is reduced. Further, this also shows that chemical ordering is not necessarily enhanced by doping with extra positive charge.

4.7 Conclusion

PMN's superstructure peaks give an X-ray diffraction pattern that, when corrected for absorption and illumination, show decreasing structure factors with increasing $|q|$. Hence, chemical ordering is the dominant feature in PMN that causes its superstructure. The positions of the oxygen atoms were further refined, and it was shown that their displacements are towards the Nb ions and away from the Mg, or ($Mg_{2/3}Nb_{1/3}$), ions. The "space charge" model is possible in pure PMN, but the "random layer" model must be present in La doped PMN. While the increase in positive charge that La provides may facilitate the growth of 1:1 chemically ordered domains, it appears that strain effects are more important. These strain effects will be considered in a different fashion in the next chapter.

The increase of chemically ordered domains caused by La doping caused more relaxor-like behavior in PMN. The increase in ordered domains also caused a much lower ferroelectric response in La-PMN, demonstrating that the chemically ordered domains are not ferroelectrically active and are distinct from the polar domains. Conversely, a decrease in ordered domain size from Ti doping caused PMN to behave less relaxor-like with a larger dielectric constant. The interference between PMN's chemically ordered and polar nanodomains is believed to be responsible for its relaxor behavior.

4.8 References

[1] G A Smolenskii, A I Agranovskaya, *Sov. Phys. -- Tech. Phys,* **3**, [7] 1380-82 (1958).

[2] J Kuwata, K Uchino and S Nomura, *Jpn. J. Appl. Phys*. **21**, 1298, 1982.

[3] N de Mathan, E Husson, G Calvarin, J R Gavarris, A W Hewat and A Morell, *J. Phys.: Condens. Matter* **3**, 8159-71 (1991).

[4] M Mulvihill, L E Cross, W Cao and K Uchino, *J. Am. Ceram. Soc.* **80**[6], 1462, (1997).

[5] N de Mathan, E Husson, G Calvarin, J R Gavarris, A W Hewat, A Morell, *J. Phys.: Condens. Matter,* **3**, 8159-71 (1991).

[6] A Verbaere, Y Piffard, Z G Ye, E Husson, *Mater. Res. Bull.,* **27**, 1227-34 (1992).

[7] S G Zhukov, V V Chernyshev, L A Aslanov, S B Vakhrushev, H Schenk, *J. Appl. Cryst.,* **28**, 385-91 (1995).

[8] G A Smolenskii, *J. Phys. Soc. Jpn.* **28**, 26-37 (1970).

[9] G A Smolenskii, A I Agranovskaya, *Sov. Phys. -- Tech. Phys,* **1**, 1429 (1959).

[10] J Chen, H M Chan and M P Harmer, *J. Am. Ceram. Soc.* **72** [4], 593-98 (1989).

[11] M A Akbas and P K Davies *J. Am. Ceram. Soc.* **80** [11], 2933 (1997).

[12] H B Krause, J M Cowley, J Wheatley, *Acta Crystallogr., Sect. A,* **35**, 1015-17 (1979).

[13] Q M Zhang, H You, M L Mulvihill, S J Jang, *Solid State Communications,* **97** [8], 693-98 (1996).

[14] A D Hilton, C A Randall, D J Barber, T R Shrout, *Ferroelectrics,* **93**, 379-86 (1989) and L A Bursill, H Qian, J-L Peng, X-D Fan, *Physica B*, **216**, 1 (1995).

[15] D D Viehland, J-F Li, *Ferroelectrics,* **158**, 381 (1994).

[16] A D Hilton, D J Barber, C A Randall and T R Shrout, *J. Mater. Sci.* **29**, 3461 (1990).

[17] L-J Lin, T-B Wu, *J. Am. Ceram. Soc.,* **73** [5], 1253-56 (1990).

[18] Commercially purchased.

[19] S L Swartz, T R Shrout, *Mater. Res. Bull.,* **17**, 1245-50 (1982).

[20] Z-G Ye, P Tissot, H Schmid, *Mater. Res. Bull.,* **25**, 739-48 (1990).

[21] The standard angle conventions for a 4-circle diffractometer are given in Busing and Levy, *Acta Cryst.* **22** 457 (1967).

[22] N de Mathan, E Husson, A Morell, *Mater. Res. Bull.*, **27**, 867-76 (1992).

[23] B E Warren, *X-Ray Diffraction*, (Addison-Wesley, Massachusetts, 1969).

[24] E Husson, M Chubb, A Morell, *Mater. Res. Bull.*, **23**, 357-61 (1988).

[25] A D Hilton, D J Barber, C A Randall, T R Shrout, *J. Mater. Sci.*, **29**, 3461-66 (1990).

[26] L E Cross, *Ferroelectrics,* **76**, 241 (1987).

[27] D J Griffiths, *Introduction to Electrodynamics*, (Prentice-Hall, New Jersey, 1989).

[28] R D Shannon, *Acta Cryst.* **A32**, 751, (1976).

[29] E V Colla, N K Yushin, D Viehland, *J. Appl. Phys.*, **83** [6] 3298 (1998).